

Toward Ultra-High Cruise Lift Coefficient Using Flapped CoFlow Jet Airfoil

Jaehyoung Jeon * Yan Ren † Gecheng Zha ‡
Dept. of Mechanical and Aerospace Engineering
University of Miami, Coral Gables, Florida 33124
E-mail: gzha@miami.edu

Abstract

Differing from the maximum lift coefficient for takeoff/landing, the cruise lift coefficient must have high aerodynamic efficiency and sufficient stall margin. Conventional 2D subsonic airfoil has the typical cruise lift coefficient C_L in the range of 0.4 to 0.6. This study introduces a 2D flapped CoFlow jet (FCFJ) airfoil to achieve a cruise lift coefficient about one order of magnitude higher to C_L of 4 with a constraint that the 2D aerodynamic efficiency should be about 50, similar to the C_L/C_D level of the baseline airfoil with no flow control. The regular CFJ airfoil applies the injection very close to leading edge at about 2-4%Chord location. The FCFJ airfoil has a long flap(60% C) with the CFJ applied inside the flap as a part of the airfoil. The research is based on validated CFD simulation, which employs a 2D RANS solver with Shear-Stress-Transport(SST) turbulence model, a third-order WENO scheme for the inviscid fluxes, second-order central differencing for the viscous terms. The regular CFJ airfoil and FCFJ airfoil are created from the baseline NACA 6421 airfoil. For a CFJ airfoil to be used at cruise conditions with high aerodynamic efficiency of $C_L/(C_D + Pc)$, both the drag and power coefficient, C_D and Pc , must be low. Applying CFJ on the flap appears to be the desired configuration to substantially increase lift coefficient and maintain very low C_D and Pc . This is benefited from the feature that applying CFJ at the region of adverse pressure gradient is the most effective and efficient. Increasing cruise lift coefficient to such a high level would bring many advantages such as reduced aircraft size/weight, increased payload, high transportation productivity, high altitude flight, and possible fixed-wing VTOL air vehicles in thin Martian atmosphere. In this study, we are able to achieve C_L of 4.17, C_L/C_D of 263.5, and $(C_L/C_D)_c$ of 48, through parametric studies on flap deflection angle, slot size, and jet momentum coefficient. The final configuration has a flap deflection angle β of 35° , the injection slot size of 0.4% C , and the jet momentum C_μ of 0.1. This 2D numerical study indicates that a cruise lift coefficient about one order of magnitude higher than conventional level is possible.

Nomenclature

CFJ	CoFlow jet
$FCFJ$	Flapped CoFlow jet

* Ph.D. Student

† Postdoc Researcher, Ph.D., AIAA member

‡ Professor, ASME Fellow, AIAA associate Fellow

$AoA(\alpha)$	Angle of attack
β	Deflection angle
LE	Leading Edge
TE	Trailing Edge
s	Wing Span length
c	Profile chord
U	Flow velocity
q	Dynamic pressure $0.5 \rho U^2$
p	Static pressure
ρ	Air density
\dot{m}	Mass flow
M	Mach number
ω	Pitching Moment
P	Pumping power
∞	Free stream conditions
C_L	Lift coefficient $L/(q_\infty S)$
C_D	Drag coefficient $D/(q_\infty S)$
C_μ	Jet momentum coef. $\dot{m}_j U_j/(q_\infty S)$
P_c	Power coefficient $L/(q_\infty S V_\infty)$
$(L/D)_c$	CFJ airfoil corrected efficiency $L/(D P/V_\infty)$
Re	Reynolds number
M	Mach number
c_p	Constant pressure specific heat
γ	Air specific heats ratio
S	Planform area of the wing
ρ_∞	Density
V_∞	Velocity
T_t	Total temperature
P_t	Total pressure
H_t	Total specific enthalpy
\dot{m}	Mass flow across the pump
Γ	Compressor total pressure ratio
∞	Subscript, stands for free stream
j	Subscript, stands for jet

1 Introduction

Cruise flight is typically the most important phase in aircraft flight envelop to achieve high mission efficiency, long range, and high transportation capacity (e.g. payload). Cruise condition thus requires aircraft to fly at high aerodynamic efficiency of C_L/C_D subject to sufficient stall margin. Typical subsonic airfoil adopts the thickness of about 15%, which provides the cruise lift coefficient in the range of 0.4 to 0.6 in order to have high aerodynamic efficiency. Thick airfoil with thickness of about 20% may have higher cruise lift coefficient of 0.7 to 1. However, thick airfoil is prone to flow separation and stall and is hence rarely used. Takeoff and landing phase of aircraft requires high lift coefficient, in particular, if a vertical or short takeoff and landing distance is desired. Conventional high lift wings with multi-element flaps achieve

maximum lift coefficient C_{Lmax} of about 2.5. However, no aircraft would cruise at such a high lift coefficient since the aerodynamic efficiency would be substantially penalized due to the excessive drag coefficient.

Active flow control (AFC) with added energy to the flow has attracted a lot of interest to increase C_{Lmax} by suppressing flow separation to increase airfoil circulation. However, using AFC for cruise is challenging because the gained benefit may not be able to offset the consumed AFC energy to let the whole aircraft system achieve a net efficiency gain. A promising AFC that shows the potential to increase cruise efficiency is the CoFlow Jet (CFJ) flow control airfoil[1, 2, 3, 4, 5, 6, 7, 8, 9, 10, 11, 12, 13, 14, 15, 16, 17]. For a regular CFJ airfoil, as shown in Fig. 1, a small amount of mass flow is withdrawn into the suction duct, pressurized and energized by a pump, and then injected near the LE tangentially to the main flow. Compared with 2D baseline airfoil, Wang and Zha[18] indicate that 2D CFJ airfoil can achieve a significantly higher cruise lift coefficient and aerodynamic efficiency defined as

$$\left(\frac{C_L}{C_D}\right)_c = \frac{C_L}{C_D + P_c} \tag{1}$$

where P_c is the CFJ required power coefficient. However, for 3D wings with finite aspect ratios, the CFJ wings can still maintain high cruise C_L , but the aerodynamic efficiency is decreased to the level of its baseline counterparts [19]. To reflect the transportation productivity of aircraft represented by the range multiplied by the gross weight, a cruise productivity efficiency is introduced as [12]:

$$\left(\frac{C_L^2}{C_D}\right)_c = \frac{C_L^2}{(C_D + P_c)} \tag{2}$$

CFJ wing can have substantially higher cruise C_L and thus greater productivity efficiency as well. Taking advantage of the CFJ wing high cruise lift coefficient and thus high suction effect on wing upper surface, Ren and Zha [20] design a tandem wing aircraft configuration that the front wing tip vortex is captured by the rear wing to enhance the overall system efficiency. With an aspect ratio of 9, the numerically simulated tandem air vehicle achieves a cruise C_L of 1.6 and $(C_L/C_D)_c$ of 13. The cruise C_L of 1.6 is beyond the reach of conventional design, which would be either stalled or suffer very high drag increase and poor aerodynamic efficiency.

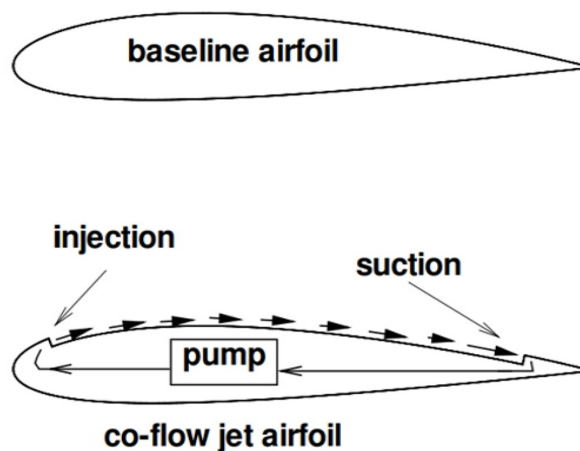


Figure 1: Sketch of CoFlow Jet airfoil

CFJ airfoil can achieve very high maximum lift coefficient exceeding the theoretical limit of $C_{Lmax} = 2\pi(1 + t/c)$ up to 15 and beyond[12, 13, 19]. However, for cruise condition, the regular CFJ configuration as shown in Fig. 1 appears to have rapid energy consumption increase when C_L is greater than 1.6[12, 21]. Even though the aerodynamic drag coefficient C_D can remain small and the pure aerodynamic lift to drag ratio C_L/C_D can be still very high, the corrected aerodynamic efficiency defined in Eq. (1) can decrease quickly with the increasing C_L when it is greater than 1.6.

The question motivating the present study is: Can we further increase cruise C_L to a level of 4 or higher? Or how to reduce the CFJ energy consumption at such a high C_L level that it can be used for cruise condition? An application to drive this motivation is to fly on Mars using fixed wing aircraft. The air density on Mars is thin and is only about 1% of that on Earth. An ultra-high cruise lift coefficient would be very important to minimize the size and the weight of the aircraft. The other application would be the ultra-high altitude flight on Earth at an altitude of 30,000 m or higher.

Cruise conditions for airfoil do not have a strict definition. We herein give a loose cruise objective and constraint for 2D CFJ airfoil: $C_L \geq 4$ with $(C_L/C_D)_c \geq 50$. The flapped CFJ airfoil studied in this paper is aimed to achieve this goal. Note that these requirements are only for 2D. When it goes to 3D finite wings, the $(C_L/C_D)_c$ is expected to substantially decrease due to the induced drag at high lift, in particular with small aspect ratio. We leave the 3D cruise effort to future work.

2 Flapped CoFlow Jet Airfoil

The concept of flapped CoFlow jet airfoil is evolved from previous applications of CFJ to deflected slipstream for VTOL hover[22], control surface flaps of supersonic aircraft[23], and transonic aircraft empennage [24]. It is also guided by the CoFlow jet flow separation mechanism study of Xu and Zha[16, 25].

The flapped CFJ(FCFJ) airfoil has a long flap with the CFJ applied inside the flap as a part of the airfoil as sketched in Fig. 2. This is different from the regular CFJ airfoil, which applies the injection very close to leading edge at about 2-4%Chord location. The advantage of the FCFJ is that the airfoil can change the angle of attack and lift coefficient by deflecting the flap without rotating the front part of the airfoil. The purpose of this paper is to demonstrate numerically that the FCFJ airfoil is a promising candidate to provide ultra-high cruise lift coefficient satisfying the objective and constraint mentioned above.

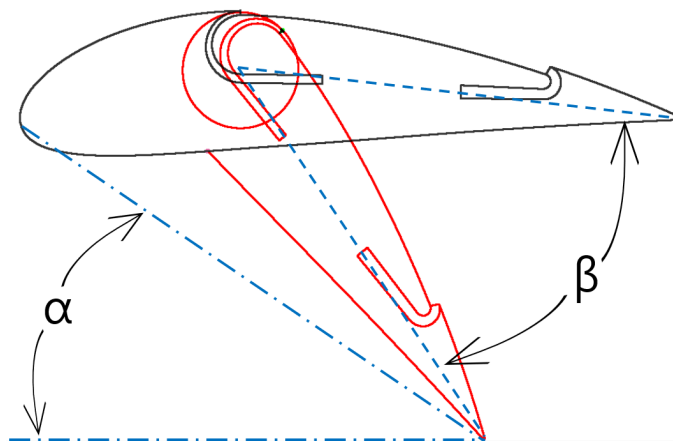


Figure 2: Sketch of flapped CFJ airfoil with the CoFlow jet applied on the flap

3 Methodology

3.1 Lift and Drag Calculation

The momentum and pressure at the injection and suction slots produce a reactionary force, which is automatically measured by the force balance in wind tunnel testing. However, for CFD simulation, the full reactionary force needs to be included. Using control volume analysis, the reactionary force can be calculated using the flow parameters at the injection and suction slot opening surfaces. Zha et al. [2] give the following formulations to calculate the lift and drag due to the jet reactionary force for a CFJ airfoil. By considering the effects of injection and suction jets on the CFJ airfoil, the expressions for these reactionary forces are given as :

$$F_{x_{cfj}} = (\dot{m}_j V_{j1} + p_{j1} A_{j1}) * \cos(\theta_1 - \alpha) - (\dot{m}_j V_{j2} + p_{j2} A_{j2}) * \cos(\theta_2 + \alpha) \quad (3)$$

$$F_{y_{cfj}} = (\dot{m}_{j1} V_{j1} + p_{j1} A_{j1}) * \sin(\theta_1 - \alpha) + (\dot{m}_{j2} V_{j2} + p_{j2} A_{j2}) * \sin(\theta_2 + \alpha) \quad (4)$$

where the subscripts 1 and 2 stand for the injection and suction respectively, and θ_1 and θ_2 are the angles between the injection and suction slot's surface and a line normal to the airfoil chord. α is the angle of attack.

The total lift and drag on the airfoil can then be expressed as:

$$D = R'_x - F_{x_{cfj}} \quad (5)$$

$$L = R'_y - F_{y_{cfj}} \quad (6)$$

where R'_x and R'_y are the surface integral of pressure and shear stress in x (drag) and y (lift) direction excluding the internal ducts of injection and suction. For CFJ wing simulations, the total lift and drag are calculated by integrating Eqs.(5) and (6) in the spanwise direction.

3.2 Jet Momentum Coefficient

The jet momentum coefficient C_μ is a parameter used to quantify the jet intensity. It is defined as:

$$C_\mu = \frac{\dot{m} V_j}{\frac{1}{2} \rho_\infty V_\infty^2 S} \quad (7)$$

where \dot{m} is the injection mass flow, V_j is the mass-averaged injection velocity, ρ_∞ and V_∞ denote the free stream density and velocity, and S is the planform area.

3.3 Micro-compressor Power Coefficient

CFJ is implemented by mounting a pumping system inside the wing that withdraws air from the suction slot and blows it into the injection slot. The power consumption is determined by the jet mass flow and total enthalpy change as the following:

$$P = \dot{m}(H_{t1} - H_{t2}) \quad (8)$$

where H_{t1} and H_{t2} are the mass-averaged total enthalpy in the injection cavity and suction cavity respectively, P is the Power required by the pump and \dot{m} the jet mass flow rate. Introducing P_{t1} and P_{t2} the mass-averaged total pressure in the injection and suction cavity respectively, the compressor efficiency η , and the total pressure ratio of the pump $\Gamma = \frac{P_{t1}}{P_{t2}}$, the power consumption is expressed as:

$$P = \frac{\dot{m}C_p T_{t2}}{\eta} (\Gamma^{\frac{\gamma-1}{\gamma}} - 1) \quad (9)$$

where γ is the specific heat ratio equal to 1.4 for air. The power coefficient is expressed as:

$$P_c = \frac{P}{\frac{1}{2}\rho_\infty V_\infty^3 S} \quad (10)$$

3.4 Aerodynamic Efficiency

The conventional wing aerodynamic efficiency is defined as:

$$\frac{C_L}{C_D} \quad (11)$$

For the CFJ wing, the ratio above still represents the pure aerodynamic relationship between lift coefficient and drag coefficient. However since CFJ active flow control consumes energy, the ratio above is modified to take into account the energy consumption of the micro-compressor. The formulation of the corrected aerodynamic efficiency for CFJ wings is:

$$\left(\frac{C_L}{C_D}\right)_c = \frac{C_L}{C_D + P_c} \quad (12)$$

where P_c is the micro-compressor power coefficient defined in Eqn. 10 and C_L and C_D are the lift and drag coefficients of the CFJ wing. If the micro-compressor power coefficient is set to 0, this formulation returns to the aerodynamic efficiency of a conventional airfoil.

A productivity efficiency parameter was introduced by Yang et al[12] It describes the capability to transport a gross weight for maximum distance at cruise

$$\left(\frac{C_L^2}{C_D}\right)_c = \frac{C_L^2}{C_D + P_c} \quad (13)$$

3.5 CFD Simulation Setup

The FASIP(Flow-Acoustics-Structure Interaction Package) CFD code is used to conduct the numerical simulation. The 2D Reynolds Averaged Navier-Stokes (RANS) equations with two-equation Shear-Stress-Transport(SST) turbulence model is used. A 3rd order WENO scheme for the inviscid flux [26, 27, 28, 29, 30, 31] and a 2nd order central differencing for the viscous terms [26, 30] are employed to discretize the Navier-Stokes equations. The low diffusion E-CUSP scheme used as the approximate Riemann solver suggested by Zha et al [27] is utilized with the WENO scheme to evaluate the inviscid fluxes. Implicit time marching method using Gauss-Seidel line relaxation is used to achieve a fast convergence rate [32]. Parallel computing is implemented to save wall clock simulation time [33].

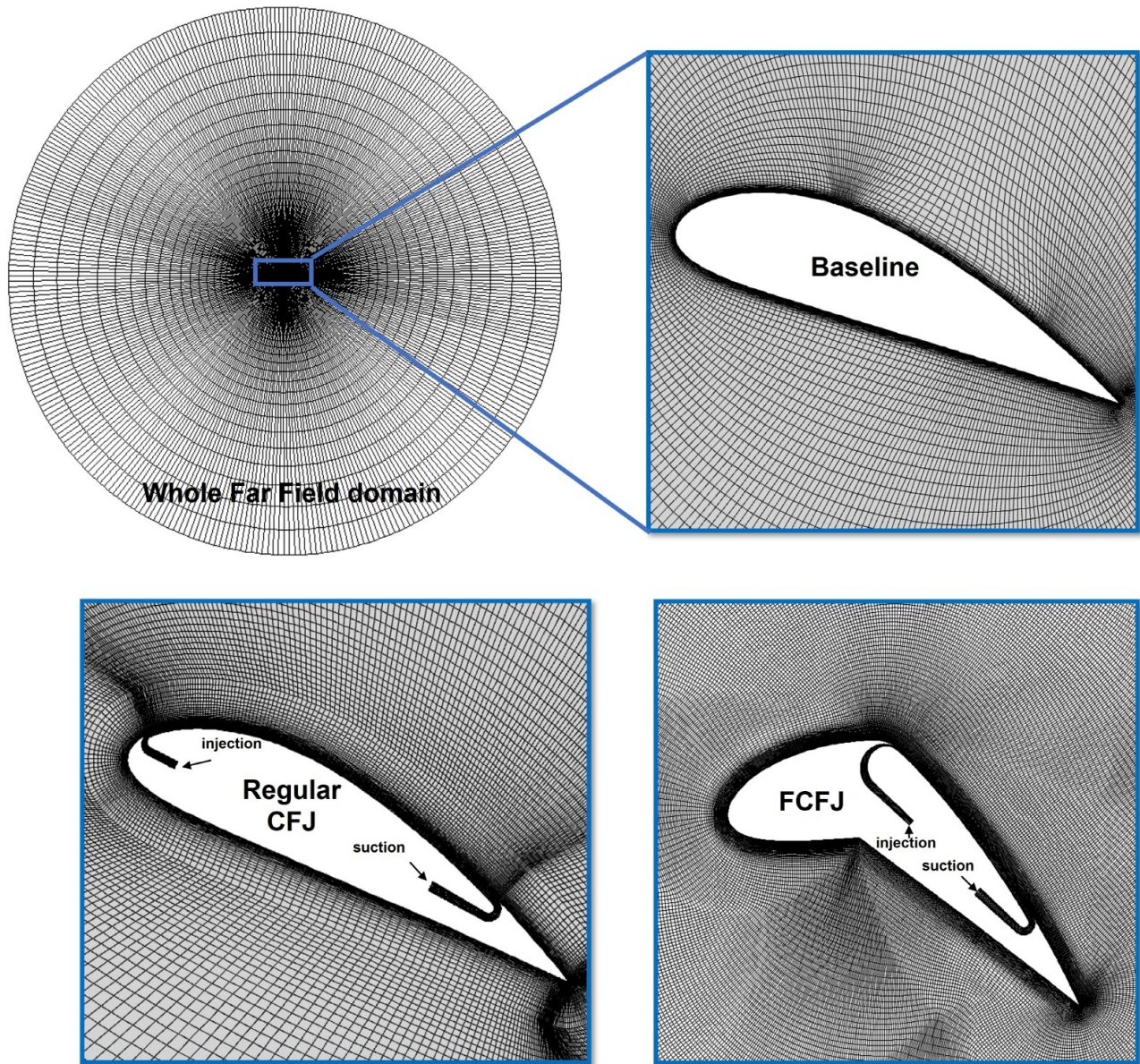


Figure 3: Computational mesh used in the current work.

3.6 Boundary Conditions

The 3rd order accuracy no slip condition is enforced on the solid surface with the wall treatment suggested in [34] to achieve the flux conservation on the wall. The far field boundary is located at 250 chord with a O-mesh topology. The computational mesh is shown in Fig. 3. Total pressure, total temperature and flow angles are specified at the upstream portion of the far field. Constant static pressure is applied at the downstream portion of the far field. The first grid point on the wing surface is placed at $y^+ \approx 1$.

4 Airfoil Geometry Parameters

Table. 1 gives the detailed parameters of the airfoils based on NACA6421 baseline with the injection and suction slot size normalized by airfoil chord length (C). The CFJ6421-SST150-SUC133-INJ065 airfoil called the regular CFJ is optimized by Lefebvre and Zha [14] for its high lift and cruise efficiency which is a reference to compare FCFJ. Flapped CFJ6421-SST150-SUC133 (FCFJ) airfoil is also developed based on the NACA 6421 airfoil which has the suction surface translation (SST) of 1.50%C and suction slot size of 1.33%C as the same as with the regular CFJ. In this study, flap deflection β is varied from 10° to 40° , and injection slot size is varied from 0.3%C to 0.8%C. The suction slot size is fixed at 1.33%C.

Table 1: Airfoil geometry parameters

Airfoil	Deflection Angle (β)	SST(%C)	INJ(%C)	SUC(%C)
NACA6421 Baseline	N/A	N/A	N/A	N/A
CFJ6421-SST150-SUC133-INJ065 (Regular CFJ)	N/A	1.5	0.65	1.33
Flapped CFJ6421-SST150-SUC133 (FCFJ)	$10^\circ - 40^\circ$	1.5	0.3 - 0.8	1.33

5 Simulated Cases

The Baseline and regular CFJ airfoils are simulated at various AoA as a comparison reference. The FCFJ airfoil is studied for its AoA and momentum coefficient effect listed in Table 2. The AoA of FCFJ is determined by the deflection angle β . The free stream Mach number is fixed at 0.17.

Table 2: Simulation cases used in the current work

Airfoil	M_∞	AoA	C_μ
NACA6421 Baseline	0.17	$2^\circ - 20^\circ$	N/A
CFJ6421-SST150-SUC133-INJ065 (Regular CFJ)	0.17	$2^\circ - 27^\circ$	0.1
Flapped CFJ6421-SST150-SUC133 (FCFJ)	0.17	$6.4^\circ - 27^\circ$	0.03 - 0.15

6 Results and Discussion

6.1 Variation of Angle of Attack and Injection Slot Size

Three airfoil configurations are simulated and compared in this study: 1)baseline NACA 6421 airfoil as shown in Fig. 4(a), 2)an optimized regular CFJ NACA-6421 airfoil designed by Wang and Zha [18] shown in Fig. 4(b), and 3)the flapped CFJ airfoil shown in Fig.4(c). The FCFJ airfoil has the flap starting at 33%C. A parametric study has been conducted to understand the characteristics of FCFJ compared to regular CFJ and baseline. The AoA range of $2^\circ \sim 20^\circ$ is studied for the Baseline airfoil, $2^\circ \sim 27^\circ$ for the Regular CFJ and, $6.4^\circ \sim 27^\circ$ for the FCFJ airfoil respectively. For this study, the Reynolds number Re is 3.48×10^6 and the Mach number is 0.17. The injection jet momentum coefficient C_μ of 0.1 is used for the two CFJ airfoils. However, C_μ of 0.1 is not the optimal value for the regular CFJ airfoil, which achieves the highest $C_L/(C_D + Pc)$ of 81 at C_μ of 0.03 at AoA of 5° [18], substantially higher than the C_L/C_D of 60 for the baseline airfoil. Since this paper is aimed at achieving ultra-high cruise lift coefficient, a high C_μ is necessary and thus is used in this section to compare the performance of the two CFJ configurations.

Fig. 4 compares the flow field Mach contours with streamlines at AoA of 20° for the baseline NACA airfoil, regular CFJ airfoil and FCFJ airfoil at C_μ of 0.1. The baseline airfoil is massively separated at AoA 20° as expected. Both the regular CFJ airfoil and FCFJ airfoil have flow well attached. For the FCFJ airfoil, the AoA of 20° corresponds to a flap deflection angle of 30° . The front part of the FCFJ airfoil is aligned with the horizontal incoming flow direction. The flow turning of the FCFJ airfoil is thus 10° greater than that of the regular CFJ airfoil assuming that the attached flow is in the direction of the trailing edge. The lift coefficient of the FCFJ airfoil is hence expected to be greater too.

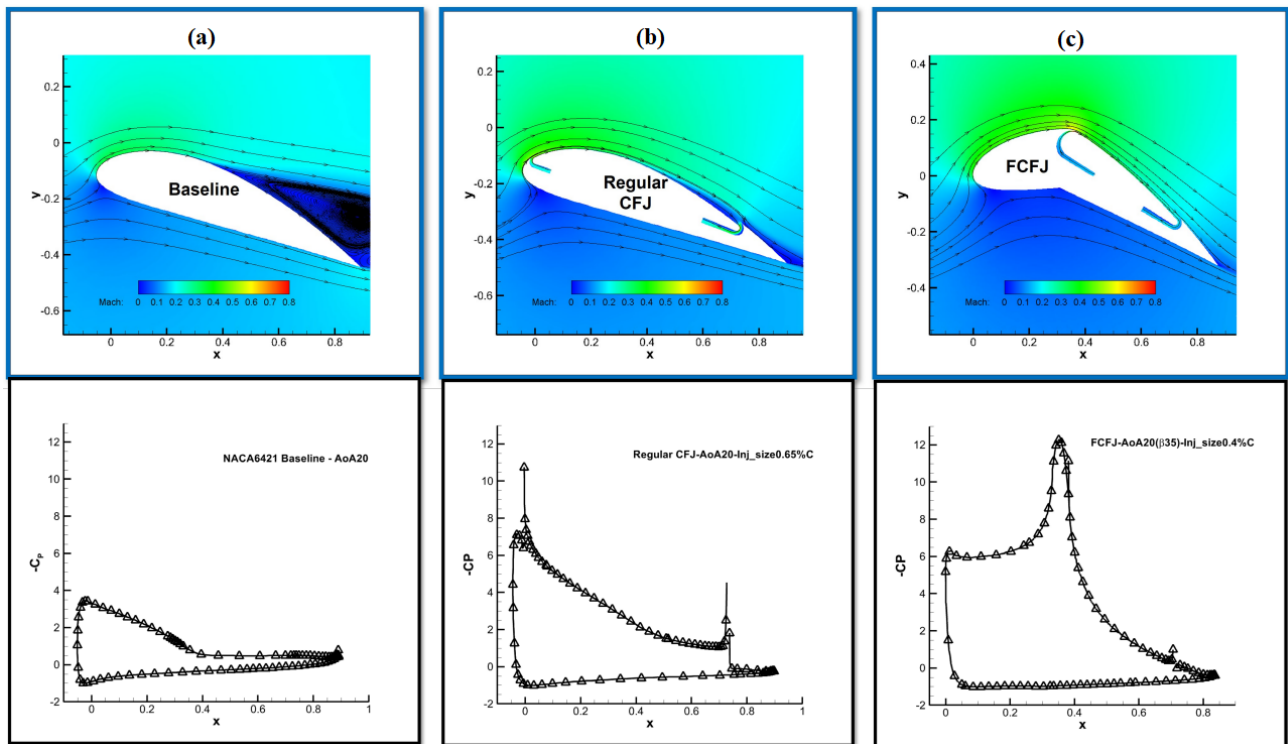


Figure 4: Mach contours and C_p distribution at AoA 20° ($\beta 30^\circ$) with $C_\mu 0.1$

The baseline NACA6421 with separated flow at AoA of 20° has a C_L of 1.52, C_L/C_D of 11.52. Fig.4 shows that both the regular CFJ and FCFJ airfoil have the flow well attached.

The surface pressure coefficient in Fig. 4 indicates that the regular CFJ airfoil has significantly higher lift coefficient than that of the baseline. Both the baseline airfoil and the regular CFJ airfoil have the typical shapes of the C_p distributions, which have the suction peak near the airfoil leading edge and the C_p value decrease due to the adverse pressure gradient. The FCFJ has a quite different C_p distribution, which has the initial suction effect at the leading edge with the C_p value very close to that of the regular CFJ airfoil. The C_p remains constant for the first 20% chord and starts to climb to a much higher suction peak at the shoulder of the deflected flap at about 40%C location, and rapidly decrease due to the very severe adverse pressure gradient on the flap suction surface. Such a C_p distribution largely increases the lift coefficient. The CFJ plays the crucial role to overcome the adverse pressure gradient and keeps the flow attached on the flap.

Fig. 5 compares the aerodynamic performance of the three airfoil configurations for C_L , C_D , P_c , and $(C_L/C_D)_c$ at different AoA and injection slot size areas. Fig. 5 shows that the regular CFJ has a maximum $(C_L/C_D)_c$ of 70 at AoA of 15° with C_L of 2.7, which is about 2.7 times higher than that of the baseline airfoil. However, when AoA is greater than 20° , the P_c and C_D of the regular CFJ airfoil increase rapidly due to separation, so does $(C_L/C_D)_c$. The C_L reaches the peak value of 3 at AoA of 20° , but the $(C_L/C_D)_c$ drops to 30, lower the constraint of 50. Further increasing C_μ to greater than 0.1 will increase the lift coefficient, but the $(C_L/C_D)_c$ goes lower than 30. This configuration is thus disqualified to achieve ultra-high cruise C_L .

To vary the AoA of the FCFJ airfoil from 6.4° to 27° , the flap deflection angle is set to 10° , 30° , 35° , and 40° Fig. 5 (a) shows that the FCFJ airfoil has the C_L continuing to increase with AoA to the level of 4.0 and beyond at the same C_μ of 0.1. At β 35° or higher, the smaller the size, the higher the C_L and the lower the C_D . This is because the injection jet has higher momentum with smaller injection slot size at higher expense of the energy consumption as shown in Fig.5 (c) Therefore, for $(C_L/C_D)_c$, the smallest size of 0.3%C shows the lowest value overall. When the injection size is 0.5%C, the P_c is low, but the FCFJ airfoil is stalled at β of 40° , with a lower $(C_L/C_D)_c$ because the flow is separated due to lacking of sufficient momentum. This is a typical behavior of CFJ airfoil. There is an optimal injection slot size to provide sufficient momentum and minimize the power consumption. Here, when the injection size is 0.4%C at β of 35° , $(C_L/C_D)_c$ is about 48 and C_L is 4.17, which is very close to the goal.

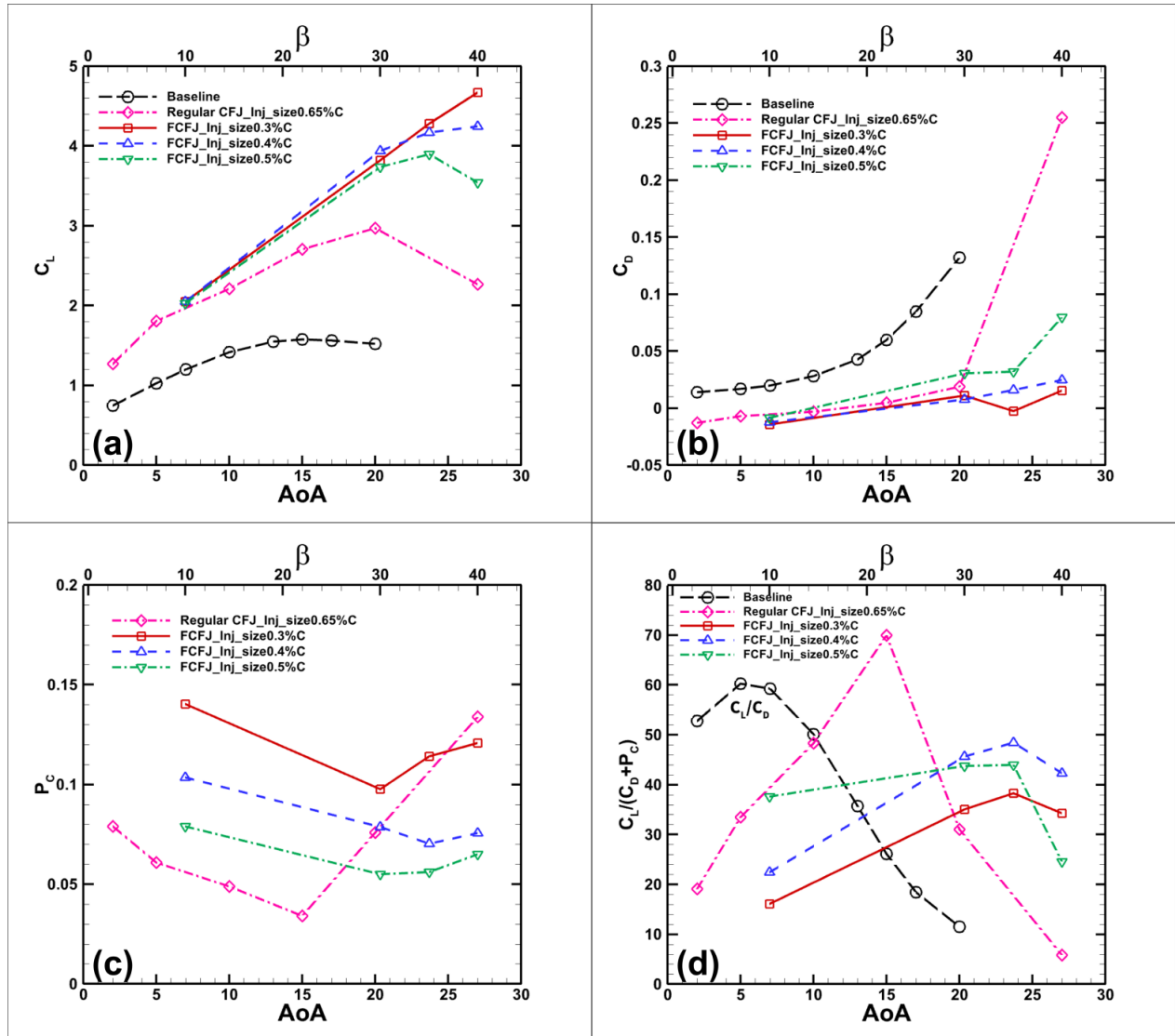


Figure 5: Aerodynamic performance of the airfoils at different AoA, (a) C_L ; (b) C_D ; (c) P_c ; (d) $(C_L/C_D)_c$

Since injection size is an important factor affecting the mass flow rate and speed of the jet, Fig. 6 presents more results with a broader range of the injection slot size at the same C_μ of 0.1. In the case of β of 10° , both the C_L and C_D are at a relatively low level and are insensitive to the injection size variation due to the low adverse pressure gradient, but the P_c decreases with the increasing slot size. The $(C_L/C_D)_c$ is thus increased from 16 to 40. When β is larger than 30° , a different tendency is shown. As the injection size increases, C_L decreases, and C_D increases rapidly. This is because the larger slot size reduce the jet momentum. But the energy required to pump the CFJ is also decreased due to the lower jet velocity and thus the energy loss until the injection slot size reaches 0.5%C, after which the CFJ does not have sufficient momentum to attach the flow and the lift thus decreases and the drag increases. Fig. 7 shows the Mach contour with different the injection size at β 35° . The slot size of 0.3%C has the flow fully attached. The 0.5% slot size still has the flow attached, but has a weak flow at the trailing edge. The 0.8%C slot size has the flow separated. The peak $(C_L/C_D)_c$ occurs at injection size of 0.4%C when β is between 30° and 40° .

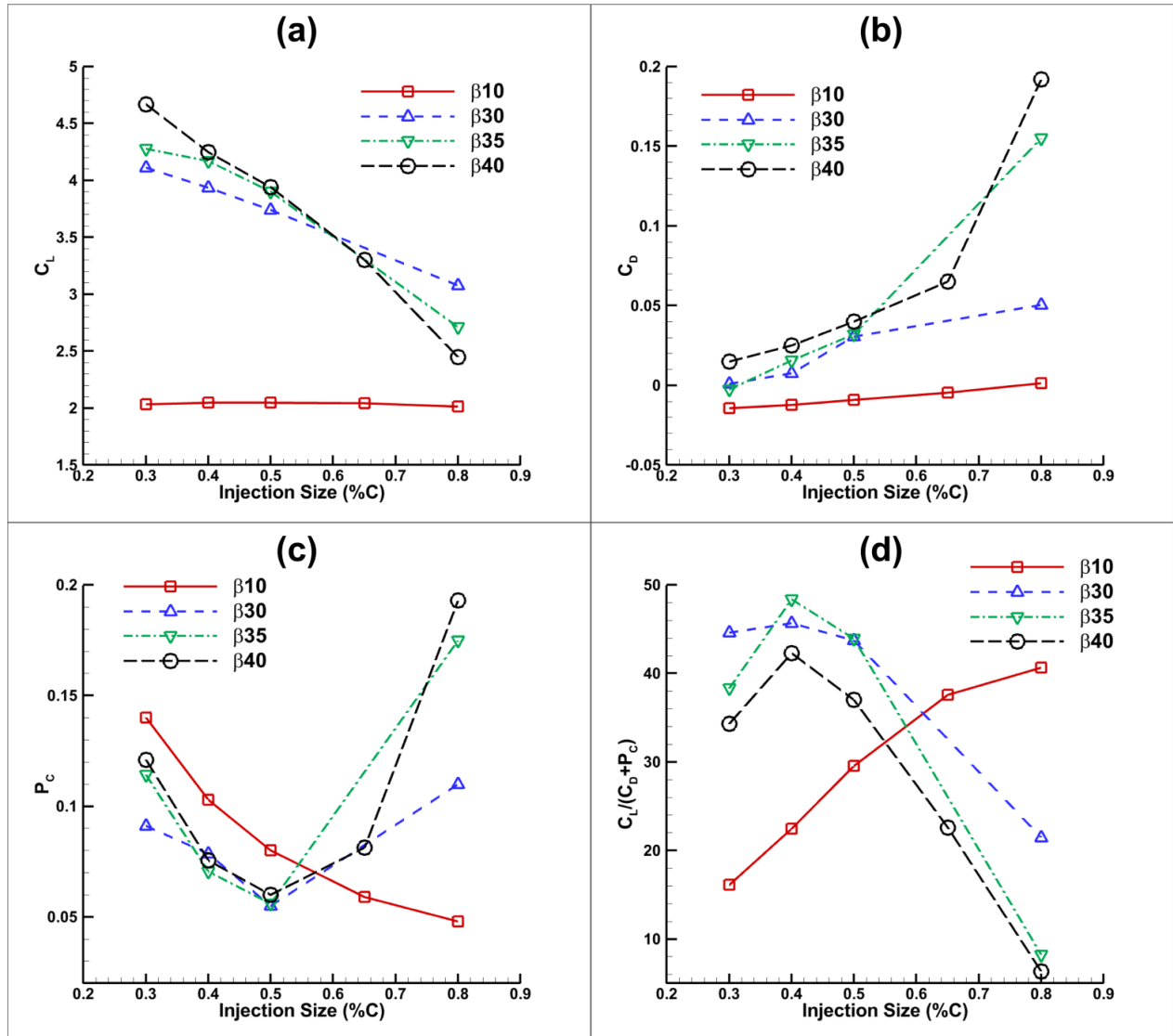


Figure 6: Aerodynamic performance of the FCFJ airfoil at different injection sizes, (a) C_L ; (b) C_D ; (c) P_c ; (d) $(C_L/C_D)_c$

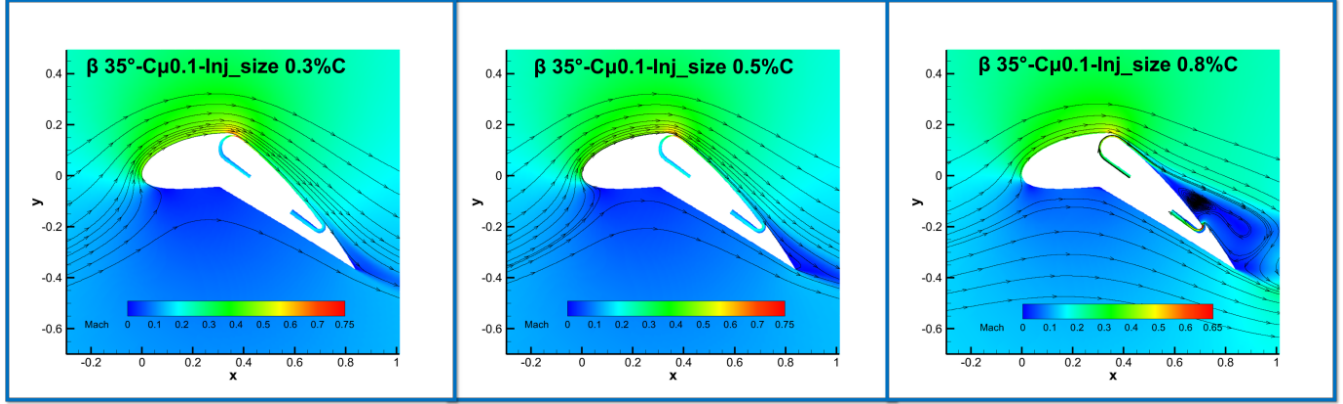


Figure 7: Mach contour of the FCFJ airfoil with different slot sizes at β of 35° , $C_\mu = 0.1$

6.2 Variation of the Jet Momentum Coefficient C_μ

C_μ represents the jet intensity as defined in Eq.7. High C_μ can achieve high aerodynamic efficiency by attaching the flow, but at the same time it can decrease $(C_L/C_D)_c$ because it increases the P_c . Fig. 8 shows the results of C_L , C_D , P_c and $(C_L/C_D)_c$ vs C_μ . In all β , as C_μ increases, C_L and P_c increase and C_D decreases. However, since the slope is different depending on β , the trend of each $(C_L/C_D)_c$ is different.

The deflection angle β of 10° has a maximum $(C_L/C_D)_c$ of 75 at C_μ 0.03 and C_L of 1.6, which is far from the target. When C_μ increases to 0.1, C_L is about 2.0, but P_c increases rapidly and $(C_L/C_D)_c$ is as low as 22. As β increases, the minimum C_μ at which separation does not occur also increases. In the case of β of 30° , a C_μ of at least 0.07 or more is required. In the case of β 40° , a minimum C_μ of 0.1 or more is required so that the flow can attach. The $(C_L/C_D)_c$ near the target value can be obtained at $C_\mu = 0.1$. If C_μ becomes too large, Mach number could reach 1 at the injection inlet and the P_c increase rapidly. Fig. 9 indicates that the case of C_μ 0.15 for β of 30° and 40° have shock wave appearance at the injection inlet. The P_c increases largely and drives the $(C_L/C_D)_c$ below 30 at C_μ 0.15. The cases at β of 30° and 35° with C_μ 0.08 to 0.1 appear satisfying the C_L of about 4 and the high $(C_L/C_D)_c$ around 50. In particular, β of 35° looks the most appropriate deflection angle for cruises because the $(C_L/C_D)_c$ does not drop below 45 even at C_μ of 0.15 and C_L up to 4.7.

The final design is summarized in the Table 3, which achieves a C_L of 4.17 and $(C_L/C_D)_c$ of 48, not completely reach the goal of 50, but very close. This study opens the possibility to achieve ultra-high cruise lift coefficient.

Table 3: The final design result

β	C_μ	INJ(%C)	SUC(%C)	C_L	C_D	C_L/C_D	$(C_L/C_D)_c$	$(C_L^2/C_D)_c$	P_c	Γ	M_{inj}	\dot{m}_j
35	0.1	0.4	1.33	4.17	0.0158	263.5	48.4	201.8	0.07	1.11	0.75	0.013

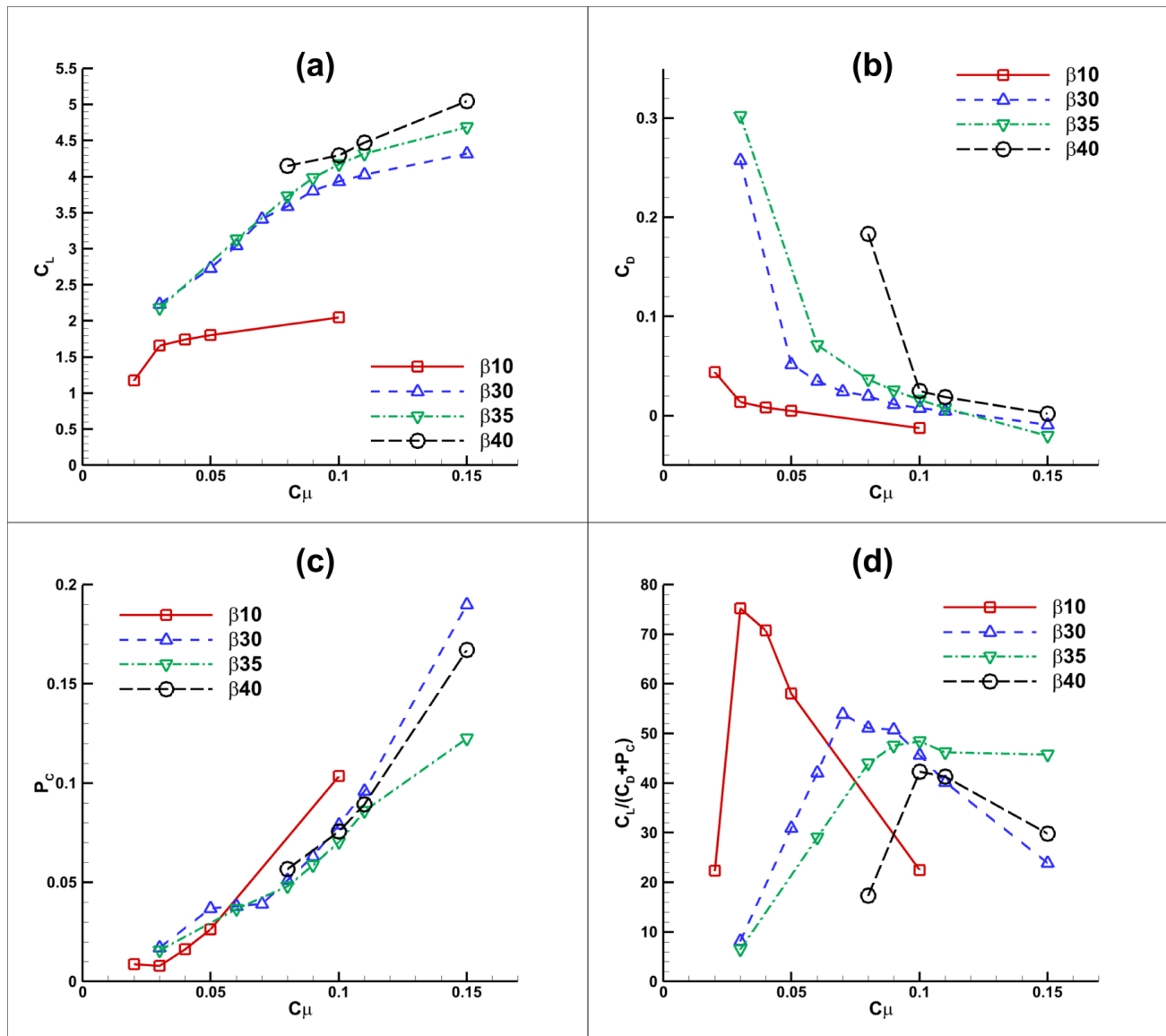


Figure 8: Aerodynamic performance of the FCFJ airfoil at different jet momentum coefficient C_{μ} , (a) C_L ; (b) C_D ; (c) P_c ; (d) $(C_L/C_D)_c$

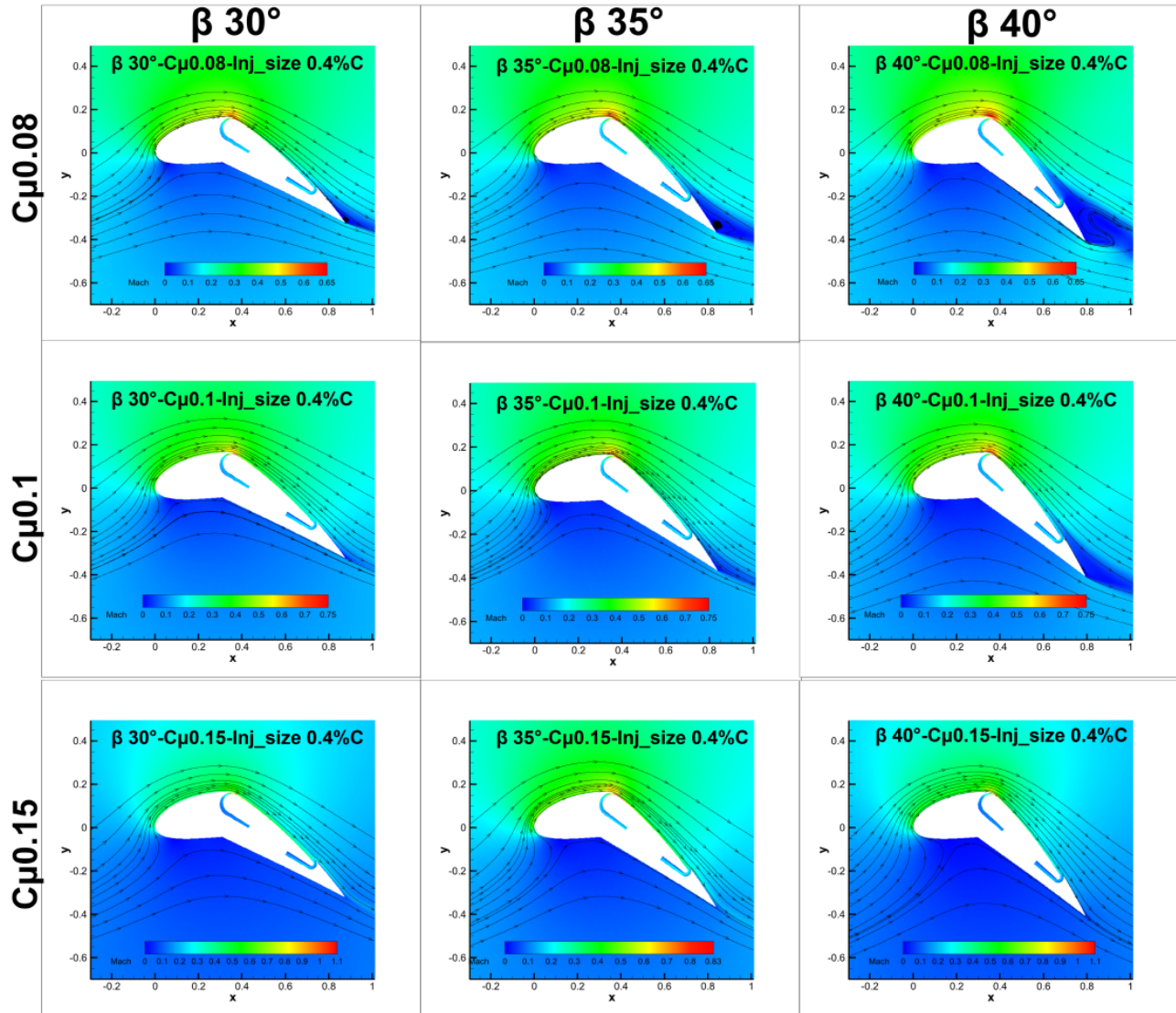


Figure 9: Mach contour for FCFJ according to β and C_μ

7 Conclusion

This paper numerically studies a 2D Flapped Coflow Jet (FCFJ) airfoil at freestream Mach number of 0.17. In the numerical results, FCFJ airfoil achieves a lift coefficient of 4.17, C_L/C_D of 263.5, and corrected aerodynamic efficiency 48. Injection size is a very sensitive design factor. A low injection size can increase the aerodynamic efficiency C_L/C_D with high C_L and low C_D , but the increased P_c may penalize the corrected aerodynamic efficiency. In this study, the $(C_L/C_D)_c$ approaches 50 at 0.4% C injection size. In addition, the momentum coefficient C_μ increases C_L and P_c and decreases C_D as C_μ increases. It is observed that the desirable C_μ is between 0.08 and 0.1 in order to obtain $(C_L/C_D)_c$ near 50. This study indicates that achieving cruise lift coefficient with an order of magnitude higher than conventional design using CFJ flapped airfoil is possible.

8 Acknowledgment

The simulations are conducted on Pegasus super computer from Center of Computer Science at University of Miami.

Disclosure: The University of Miami and Dr. Gecheng Zha may receive royalties for future commercialization of the intellectual property used in this study. The University of Miami is also equity owner in CoFlow Jet, LLC, licensee of the intellectual property used in this study.

References

- [1] G.-C. Zha and D. C. Paxton, "A Novel Flow Control Method for Airfoil Performance Enhancement Using Co-Flow Jet." *Applications of Circulation Control Technologies*, Chapter 10, p. 293-314, Vol. 214, Progress in Astronautics and Aeronautics, AIAA Book Series, Editors: Joslin, R. D. and Jones, G.S., 2006.
- [2] G.-C. Zha, W. Gao, and C. Paxton, "Jet Effects on Co-Flow Jet Airfoil Performance," *AIAA Journal*, No. 6,, vol. 45, pp. 1222–1231, 2007.
- [3] G.-C. Zha, C. Paxton, A. Conley, A. Wells, and B. Carroll, "Effect of Injection Slot Size on High Performance Co-Flow Jet Airfoil," *AIAA Journal of Aircraft*, vol. 43, 2006.
- [4] G.-C. Zha, B. Carroll, C. Paxton, A. Conley, and A. Wells, "High Performance Airfoil with Co-Flow Jet Flow Control," *AIAA Journal*, vol. 45, 2007.
- [5] Wang, B.-Y. and Haddoukessouni, B. and Levy, J. and Zha, G.-C., "Numerical Investigations of Injection Slot Size Effect on the Performance of Co-Flow Jet Airfoil," *Journal of Aircraft*, vol. Vol. 45, No. 6., pp. pp.2084–2091, 2008.
- [6] B. P. E. Dano, D. Kirk, and G.-C. Zha, "Experimental Investigation of Jet Mixing Mechanism of Co-Flow Jet Airfoil." AIAA-2010-4421, 5th AIAA Flow Control Conference, Chicago, IL, 28 Jun - 1 Jul 2010.
- [7] B. P. E. Dano, G.-C. Zha, and M. Castillo, "Experimental Study of Co-Flow Jet Airfoil Performance Enhancement Using Micro Discreet Jets." AIAA Paper 2011-0941, 49th AIAA Aerospace Sciences Meeting, Orlando, FL, 4-7 January 2011.
- [8] A. Lefebvre, B. Dano, W. Bartow, M. Fronzo, and G. Zha, "Performance and energy expenditure of coflow jet airfoil with variation of mach number," *Journal of Aircraft*, vol. 53, no. 6, pp. 1757–1767, 2016.
- [9] A. Lefebvre, G-C. Zha, "Numerical Simulation of Pitching Airfoil Performance Enhancement Using Co-Flow Jet Flow Control," *AIAA paper 2013-2517*, June 2013.
- [10] A. Lefebvre, G-C. Zha, "Cow-Flow Jet Airfoil Trade Study Part I : Energy Consumption and Aerodynamic Performance," *Proceedings of the AIAA Flow Control Conference*, June 2014.
- [11] A. Lefebvre, G-C. Zha, "Cow-Flow Jet Airfoil Trade Study Part II : Moment and Drag," *Proceedings of the AIAA Flow Control Conference*, June 2014.

- [12] Yunchao Yang, Gecheng Zha, "Super-Lift Coefficient of Active Flow Control Airfoil: What is the Limit?," *AIAA Paper 2017-1693, AIAA SCITECH2017, 55th AIAA Aerospace Science Meeting, Grapevine, Texas, 9-13 January 2017*, 2017.
- [13] Gecheng Zha, Yunchao Yang, Yan Ren, Brendan McBreen, "Super-Lift and Thrusting Airfoil of Coflow Jet Actuated by Micro-Compressors," *AIAA Paper-2018-3061, AIAA AVIATION Forum 2018, Flow Control Conference, June 25-29, 2018*.
- [14] Lefebvre, A. and Zha, G.-C., "Trade Study of 3D Co-Flow Jet Wing for Cruise Performance." *AIAA Paper 2016-0570, AIAA SCITECH2016, AIAA Aerospace Science Meeting, San Diego, CA, 4-8 January 2016*.
- [15] Kewei Xu, Gecheng Zha, "High Control Authority 3D Aircraft Control Surfaces Using Co-Flow Jet," *AIAA Journal of Aircraft*, 2020.
- [16] Kewei Xu, Gecheng Zha, "System energy benefit using co-flow jet active separation control for a serpentine duct," *Elsevier Journal of Aerospace Science and Technology 128 (2022)107746*, <https://doi.org/10.1016/j.ast.2022.107746>, 2022.
- [17] Kewei Xu, Yan Ren, Gecheng Zha, "Numerical Analysis of Energy Expenditure for Co-Flow Wall Jet Separation Control," *AIAA Paper 2022-1547, AIAA Scitech Forum, January 3-7, 2022*.
- [18] Yang Wang and Gecheng Zha, "Study of Mach Number Effect for 2D Co-Flow Jet Airfoil at Cruise Conditions," *AIAA Paper 2019-3169, AIAA Aviation 2019 Forum, 17-21 June 2019, Dallas, Texas, 2019*.
- [19] Yang Wang and Gecheng Zha, "Study of Mach Number Effect for 3D Co-Flow Jet Wings at Cruise Conditions," *AIAA Paper 2020-0045, AIAA SciTech Forum, 6-10 January 2020, Orlando, FL, 2020*.
- [20] Yan Ren, Gecheng Zha, "Performance Enhancement by Tandem Wings Interaction of CoFlow Jet Aircraft," *AIAA Paper 2021-1823, AIAA SciTech Forum, 11-15; 19-21 January 2021, VIRTUAL EVENT*, 2021.
- [21] Yang Wang, Yunchao Yang and Gecheng Zha, "Study of Super-Lift Coefficient of Co-Flow Jet Airfoil and Its Power Consumption," *AIAA Paper 2019-3652, AIAA Aviation 2019 Forum, 17-21 June 2019, Dallas, Texas*, 2019.
- [22] Ren. Y. and Zha, G.-C., "Simulation of 2D CoFlow Jet Deflected Slipstream VTOL Transition Transient Flows," *10th Annual Electric VTOL Symposium, Mesa, AZ, Jan. 24-26, 2023*.
- [23] Zhijin Lei, Gecheng Zha, "Lift Enhancement for Supersonic Delta Wing at Low Speed Using CoFlow Jet," *AIAA Paper 2021-2559, AIAA AVIATION Forum, August 2-6, 2021*.
- [24] Kewei Xu, Gecheng Zha, "3D Aircraft Control Surface Enabled by Co-Flow Jet Flap," *AIAA Paper-2022-3889, AIAA AVIATION Forum, June 27-July 1, Chicago, IL Virtual*, 2022.
- [25] Kewei Xu, Yan Ren, and Gecheng Zha, "Separation Control by Co-Flow Wall Jet," *AIAA Paper 2021-2946, AIAA AVIATION Forum, August 2-6, 2021*.
- [26] Y.-Q. Shen and G.-C. Zha, "Large Eddy Simulation Using a New Set of Sixth Order Schemes for Compressible Viscous Terms ," *Journal of Computational Physics*, vol. 229, pp. 8296–8312, 2010.
- [27] Zha, G.C., Shen, Y.Q. and Wang, B.Y., "An improved low diffusion E-CUSP upwind scheme ," *Journal of Computer and Fluids*, vol. 48, pp. 214–220, Sep. 2011.

- [28] Y.-Q. Shen and G.-Z. Zha , “Generalized finite compact difference scheme for shock/complex flowfield interaction,” *Journal of Computational Physics*, vol. doi:10.1016/j.jcp.2011.01.039, 2011.
- [29] Shen, Y.-Q. and Zha, G.-C. and Wang, B.-Y., “ Improvement of Stability and Accuracy of Implicit WENO Scheme,” *AIAA Journal*, vol. 47, No. 2, pp. 331–344, 2009.
- [30] Shen, Y.-Q. and Zha, G.-C. and Chen, X.-Y., “ High Order Conservative Differencing for Viscous Terms and the Application to Vortex-Induced Vibration Flows,” *Journal of Computational Physics*, vol. 228(2), pp. 8283–8300, 2009.
- [31] Shen, Y.-Q. and Zha, G.-C. , “ Improvement of the WENO Scheme Smoothness Estimator,” *International Journal for Numerical Methods in Fluids*, vol. DOI:10.1002/flid.2186, 2009.
- [32] G.-C. Zha and E. Bilgen, “Numerical Study of Three-Dimensional Transonic Flows Using Unfactored Upwind-Relaxation Sweeping Algorithm,” *Journal of Computational Physics*, vol. 125, pp. 425–433, 1996.
- [33] B.-Y. Wang and G.-C. Zha, “A General Sub-Domain Boundary Mapping Procedure For Structured Grid CFD Parallel Computation,” *AIAA Journal of Aerospace Computing, Information, and Communication*, vol. 5, No.11, pp. 2084–2091, 2008.
- [34] Y.-Q. Shen, G.-C. Zha, and B.-Y. Wang, “Improvement of Stability and Accuracy of Implicit WENO Scheme ,” *AIAA Journal*, vol. 47, pp. 331–344, 2009.